THE JOURNAL OF PHYSICAL CHEMISTRY A

Article

pubs.acs.org/JPCA

Synthesis, Electrochemistry, and Excited-State Properties of Three Ru(II) Quaterpyridine Complexes

Jennifer A. Rudd, M. Kyle Brennaman, Katherine E. Michaux, Dennis L. Ashford, Royce W. Murray, and Thomas. J. Meyer*

Department of Chemistry, University of North Carolina at Chapel Hill, CB 3290, Chapel Hill, North Carolina 27599-3290, United States

Supporting Information

ABSTRACT: The complexes $[Ru(qpy)LL']^{2+}$ (qpy = 2,2′:6′,2″:6″,2‴-quaterpyridine), with **1**: L = acetonitrile, L′= chloride; **2**: L = L′= acetonitrile; and **3**: L = L′= vinylpyridine, have been prepared from $[Ru(qpy)(Cl)_2]$. Their absorption spectra in CH_3CN exhibit broad metal-to-ligand charge transfer (MLCT) absorptions arising from overlapping $^1A_1 \rightarrow {}^1$MLCT transitions. Photoluminescence is not observed at room temperature, but all three are weakly emissive in 4:1 ethanol/methanol glasses at 77 K with broad, featureless emissions observed between 600 and 1000 nm consistent with MLCT phosphorescence. Cyclic voltammograms in CH_3CN reveal the expected $Ru^{III/II}$ redox couples. In 0.1 M trifluoroacetic acid (TFA), **1** and **2** undergo aquation to give $[Ru^{II}(qpy)(OH_2)_2]^{2+}$, as evidenced by the appearance of waves for the couples $[Ru^{III}(qpy)(OH_2)_2]^{3+}/[Ru^{II}(qpy)(OH_2)_2]^{2+}$, $[Ru^{IV}(qpy)(O)(OH_2)]^{2+}/[Ru^{III}(qpy)(OH_2)_2]^{3+}$, and $[Ru^{VI}(qpy)(O)_2]^{2+}/[Ru^{IV}(qpy)(O)(OH_2)]^{2+}$ in cyclic voltammograms.

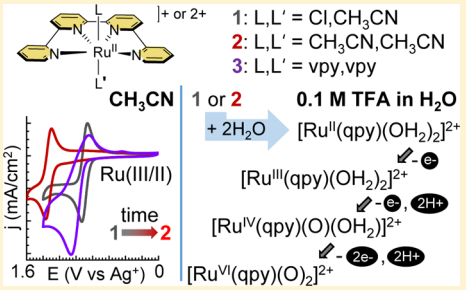

INTRODUCTION

The molecular approach to artificial photosynthesis holds significant promise for harnessing solar energy to generate solar fuels.[1−7] A primary target is water splitting to dioxygen with the released four electrons and four protons used at the reductive electrode to generate hydrogen or to reduce carbon dioxide. Challenges in water oxidation catalysis stem from the thermodynamic and mechanistic requirements for O···O bond formation and the $4e^-/4H^+$ nature of the reaction. Despite these hurdles, multiple molecular water oxidation catalysts (WOCs) have been developed[8] including a plethora of Ru(II) polypyridyl complexes with carboxylate, carbene, and (benz)imidazole ligands.[9,10] Although the majority of catalysts have a coordinated water bound as a ligand to Ru(II), coordinatively saturated examples have also been reported.[11−16] Ru(II) complexes with a tetradentate ligand have been shown to be efficient photosensitizers for dye-sensitized solar cells,[17] with the same ligand used for water oxidation.[18] Recently Thummel and coworkers reported that $[Ru(dpp)(pic)_2]$ (dpp = 2,9-di(pyrid-2′-yl)-1,10-phenanthroline; pic is picoline, *p*-methylpyridine) is an active catalyst with Ce^{IV} as the oxidant.[15] Lau et al. demonstrated that $[Ru(qpy)(pic)_2]^{2+}$ (qpy = 2,2′:6′,2″:6″,2‴-quaterpyridine) is oxidized by Ce^{IV} to form a qpy-*N*,*N*‴- dioxide complex, which acts as a water oxidation catalyst.[19] The bis-aqua form of this complex has been studied by Che et al., and its properties as an alcohol oxidation catalyst have been reported.[20]

We report here the synthesis and characterization of salts of three new water oxidation candidates based on the {Ru(qpy)} motif, $[Ru(qpy)(CH_3CN)Cl]^+$ (**1**), $[Ru(qpy)(CH_3CN)_2]^{2+}$ (**2**), and $[Ru(qpy)(vpy)_2]^{2+}$ (**3**) with vpy = *para*-vinylpyridine (Scheme 1). Complexes **1** and **2** were the initial targets as synthetic precursors due to their facile syntheses and the lability of the coordinated acetonitrile ligand upon oxidation to Ru(III)[21] which provides an efficient route to the diaqua catalyst reported by Che et al. In complex **3**, the addition of the

Scheme 1. Structures of the Ruthenium Quaterpyridine Complexes 1, 2, and 3

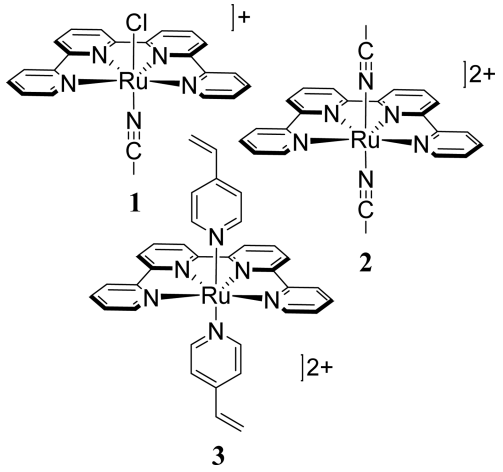

Received: January 11, 2016
Revised: February 17, 2016
Published: February 18, 2016

DOI: 10.1021/acs.jpca.6b00317
J. Phys. Chem. A 2016, 120, 1845−1852

trans-vpy ligands provides a basis for forming redox-active films on conductive substrates by reductive electropolymerization.[21−24] The synthetic procedure is outlined in Scheme S1.

EXPERIMENTAL SECTION

The ligand qpy and the complex $[Ru(qpy)(Cl)_2]$ were prepared according to literature procedures for the analogous dpp[25] and $[Ru(dpp)(Cl)_2]$[26] compounds previously reported by Thummel et al., respectively. $[RuCl_3]$, dry solvents from Sigma-Aldrich, and chromatography solvents from Fisher Chemicals were all used as received. Size exclusion chromatography was carried out using Sephadex LH-20. ^{1}H NMR spectra were recorded with a 600 MHz Bruker spectrometer with chemical shifts referenced to the solvent residue peak. Electronic absorption spectra were collected on an Agilent 8453 UV−vis-NIR spectrophotometer and corrected for the background spectrum of the solvent. Elemental analyses were performed by Atlantic Microlabs (Norcross, GA).

Cyclic voltammetry was performed on 1 mM solutions of each complex by using a CH Instruments 660A potentiostat outfitted with a conventional three electrode setup consisting of a glassy carbon working electrode, a platinum wire auxiliary electrode, and a reference electrode. For aqueous 0.1 M trifluoroacetic acid solutions, the reference electrode was Ag/AgCl (BASi, 3 M NaCl, 0.209 V vs NHE). For acetonitrile solutions, the same Ag/AgCl reference electrode was used and 0.1 M tetrabutylammonium hexafluorophosphate was added as supporting electrolyte.

Steady-State Emission at 77 K. For each complex, a millimolar amount was dissolved in 4 mL of a 4:1 ethanol/methanol mixed solvent. Each solution was added to a separate NMR tube (quartz, 5 mm diameter, 1 mm wall thickness, Wilmad). Once filled with solution, each NMR tube was inserted into a coldfinger dewar with sufficient liquid nitrogen to completely submerge the solution. *Safety note: Consult the MSDS and take adequate precautions, for example, safety goggles and cryogenic gloves when handling liquid nitrogen to avoid severe burns.* Care was taken to ensure that a crack-free alcohol glass resulted upon cooling to 77 K. If cracks were observed, the solution was warmed and then cooled again until a high-quality glass was achieved. Luminescence spectra (600−950 nm, every 1 nm, 0.2 s integration time, three averages) were collected at 77 K by inserting the NMR tube/liquid nitrogen coldfinger dewar into an Edinburgh FLS-920 emission spectrophotometer equipped with a thermoelectrically cooled (−20 °C) photomultiplier tube (R2658P, Hamamatsu). Visible excitation was provided by a 450 W Xe source focused into a monochromator. Spectral bandwidth for both emission and excitation monochromators was fixed at 10 nm. A 320 nm long pass filter was placed in the path of the excitation beam just before the sample to avoid UV photoexcitation arising from second-order grating effects. A 570 nm long pass filter was placed between the sample and the emission monochromator to avoid stray light and second-order grating effects from visible excitation light scattered from the curved surfaces of the glassware. Resulting spectra were corrected for the transmission of both the 570 nm long pass filter and the spectral response of the system. Spectral correction factors were collected in a separate experiment using a NIST-traceable standard tungsten lamp. Spectra of the mixed alcohol glass, free of complex, were subtracted from those with complex. Although a coldfinger dewar was used, a steady stream of gas nitrogen bubbles was generated as liquid nitrogen boiled. This phenomenon led to increased noise in blank-subtracted spectra despite efforts to minimize its severity. Furthermore, quantitative blank subtraction was problematic, owing both to boiling nitrogen and to small variations in sample placement. Excitation light intensity fluctuations were monitored by directing a small fraction of the excitation beam, via a beamsplitter, onto a Si reference detector. The signal from the Si reference detector was used to correct for any excitation light intensity fluctuations. To prevent condensation buildup on the outside of the liquid nitrogen dewar, we used tygon tubing to direct gas nitrogen into the instrument to minimize water vapor. Data shown are the result of at least two trials of sample preparation and data collection. Aliquots from independent syntheses of the same complex were used as an additional check of data and sample integrity.

Photoluminescence Spectral Fitting. In preparation for spectral fitting, observed emission spectra corrected for instrument spectral response were expressed in wavenumbers with intensities converted to units of quanta per second by multiplication by the square of the wavelength.[27] The transformed spectra were fit to the single average mode, Franck−Condon expression in eq 1.[28−32]

$$I(\tilde{\nu}) = \sum_{\nu_M=0}^{\infty} \left\{ \left(\frac{E_0 - \nu_M \hbar\omega_M}{E_0} \right)^3 \left(\frac{{S_M}^{\nu_M}}{\nu_M!} \right) \times \exp\left[-4\ln(2) \left(\frac{\tilde{\nu} - E_0 + \nu_M \hbar\omega_M}{\Delta\tilde{\nu}_{0,1/2}} \right)^2 \right] \right\} \quad (1)$$

In this expression, E_0 is the energy difference between the lowest energy ^{3}MLCT excited state and the ground state, $\Delta\tilde{\nu}_{0,1/2}$ is the full width at half-maximum (fwhm) of the Gaussian-broadened 0−0 vibronic component, $\hbar\omega_M$ is the quantum vibrational energy spacing of the single acceptor mode of medium frequency, and S_M is the Huang−Rhys factor or electron-vibrational coupling constant, which is a measure of the change in equilibrium normal coordinate between excited and ground state. With $\hbar\omega_M$ fixed at 1350 cm^{-1}, the three variable parameters E_0, $\Delta\tilde{\nu}_{0,1/2}$, and S_M were iteratively optimized until a global minimum was reached by the use of a trust-region-reflective, least-squares algorithm carried out with custom software written and executed in MatLab (The MathWorks, version R2014b). The summation included 11 vibrational levels ($\nu_M = 0 \rightarrow 10$).

Time-Resolved Photoluminescence at 77 K. Time-correlated single photon counting (TCSPC) measurements were obtained by using the Edinburgh FLS-920 spectrophotometer previously mentioned. Rather than Xe lamp excitation, an EPL-445 pulsed diode laser (444 nm, ∼100 ps fwhm, 2 us or 5 us as needed pulse period, ∼20 nJ/pulse, 2 mm beam diameter) was used as the excitation source. The instrument response function was collected by tuning the emission monochromator close to the laser wavelength and was found to be ∼5 ns fwhm. The TCSPC electronics (PCS900 and TCS900 data acquisition boards) were set to define 0.9766 or 1.221 ns/channel over either a 1, 2, or 5 us window, as needed. The timing sequences were begun by electronic pulses triggered by the laser pulses, while the stop pulses were triggered by detected photons. Care was taken to ensure that stop pulses were recorded for <5% of start pulses to avoid counting/timing errors. First-order rate constants were determined by using the tail-fitting algorithm in the Edinburgh

DOI: 10.1021/acs.jpca.6b00317
J. Phys. Chem. A 2016, 120, 1845−1852

F900 software by including only data outside the time window of the instrument response function. At least 10 000 counts were accumulated in the channel with the maximum counts. Data shown are the result of at least two trials of sample preparation and data collection. Aliquots from independent syntheses of the same complex were used as an additional check of data and sample integrity.

Synthesis. For reference, the protons of the qpy ligand are lettered from a−g, as shown in Scheme S2.

*[Ru(qpy)(CH$_3$CN)Cl][BF$_4$] (**1**).* 60 mg (0.12 mmol) of [Ru(qpy)(Cl)$_2$] and 24.2 mg (1 equiv, 0.12 mmol) of AgBF$_4$ were placed into a flask equipped with a stir bar and evacuated and refilled with N$_2$ three times. Following the addition of 15 mL of dry acetonitrile, the reaction was heated at reflux overnight. The solution was cooled to room temperature and filtered, and the solvent was removed in vacuo. The complex was purified using size exclusion chromatography with 1:1 acetonitrile/water as eluent. The purple fraction was collected and dried yielding a purple powder. Yield: 35 mg, 49.0%. ^{1}H NMR (acetonitrile-d_3, 600 MHz): δ 9.55−9.51 (m, 1H, H^a), 8.42−8.37 (m, 2H, H^{d+e}), 8.28 (d, J = 8.0 Hz, 1H, H^g), 8.21 (td, J = 7.8, 1.6 Hz, 1H, H^c), 7.98 (dd, J = 8.0, 8.0 Hz, 1H, H^f), 7.86 (ddd, J = 7.6, 5.2, 1.3 Hz, 1H, H^b). ESI−MS: [Ru(qpy)(CH$_3$CN)$_2$(BF$_4$)]$^+$ 581.32 (calc. 581.08), [M]$^+$ 575.33 (calc. 575.03), [M-BF$_4$]$^+$ 488.27 (488.02), [Ru(qpy)(CH$_3$CN)$_2$]$^{2+}$ 247.04 (calc. 247.04). Anal. Calcd for C$_{22}$H$_{17}$BClF$_4$N$_5$Ru·3H$_2$O: C, 42.02; H, 3.69; N, 11.14. Observed: C, 41.61; H, 3.53; N, 11.38.

*[Ru(qpy)(CH$_3$CN)$_2$][BF$_4$]$_2$ (**2**).* 60 mg (0.12 mmol) [Ru(qpy)(Cl)$_2$] and 55 mg (excess, 0.28 mmol) AgBF$_4$ were placed in a flask equipped with a stir bar. The flask was evacuated and refilled with N$_2$ three times. Following the addition of 15 mL of dry acetonitrile, the reaction was heated at reflux overnight. The solution was cooled to room temperature and filtered, and the solvent removed in vacuo. The complex was purified using size exclusion chromatography with 1:1 acetonitrile/water as eluent. The second fraction from the column was collected and the solvent was removed in vacuo, affording a dark red powder. Yield: 53.0 mg, 83.2%. ^{1}H NMR (acetonitrile-d_3, 600 MHz): δ 9.44−9.37 (d, J = 1H, H^a), 8.46−8.42 (m, 2H, H^{d+e}), 8.36 (d, J = 8.0 Hz, 1H, H^g), 8.29 (td, J = 7.8, 1.6 Hz, 1H, H^c), 8.18 (t, J = 8.1 Hz, 1H, H^f), 7.89 (ddd, J = 7.7, 5.2, 1.3 Hz, 1H, H^b). ESI−MS: [M-BF$_4$]$^+$ 581.32 (calc. 581.08), [M-2BF$_4$]$^{2+}$ 247.04 (calc. 247.04). Anal. Calcd for C$_{24}$H$_{20}$BF$_4$N$_6$Ru·3H$_2$O·CH$_3$CN: C, 40.97; H, 3.84; N, 12.86. Observed: C, 41.40; H, 3.40; N, 12.75.

*[Ru(qpy)(vpy)$_2$][Cl]$_2$ (**3**).* 60 mg (0.12 mmol) [Ru(qpy)(Cl)$_2$] and 0.65 mL of (50 equiv, 6.0 mmol, 654 mg) *para*-vinylpyridine were heated at reflux in 10 mL of ethanol and 3 mL of H$_2$O for 2 days. The reaction was then allowed to cool to room temperature and the solvent wasremoved in vacuo. The resulting solid was dissolved in 1:1 methanol/water and purified using size exclusion chromatography with 1:1 methanol/water as the eluent. The dark purple fraction was collected and the solvent was removed in vacuo, affording a dark purple powder. Yield: 60.0 mg, 73.4%. ^{1}H NMR (acetonitrile-d_3, 600 MHz) δ 10.03 (dd, J = 5.3, 1.6 Hz, 1H, H^a), 8.67 (d, J = 8.1 Hz, 1H, H^b), 8.34 (d, J = 8.0 Hz, 1H, H^g), 8.24 (dd, J = 7.8, 1.2 Hz, 1H, H^c), 8.17−8.06 (m, 2H, H^{d+e}), 7.94 (ddt, J = 7.4, 5.4, 2.4 Hz, 1H, H^f), 7.92−7.87 (m, 2H, H^{py}), 7.10−7.00 (m, 2H, H^{py}), 6.49 (dd, J = 17.6, 10.9 Hz, 1H, H^{vinyl}), 5.91 (d, J = 17.6 Hz, 1H, H^{vinyl}), 5.46 (d, J = 10.9 Hz, 1H, H^{vinyl}). ESI−MS: [M-Cl]$^+$ 657.25 (calc. 657.11), [M-L-Cl]$^+$ 552.29 (calc. 552.05), [M-2Cl]$^{2+}$ 311.17 (calc. 311.07). Anal. Calcd for C$_{34}$H$_{28}$ClN$_6$Ru·4H$_2$O: C, 53.68; H, 5.00; N, 10.98. Observed: C, 53.41; H, 5.00; N, 10.98.

RESULTS AND DISCUSSION

Synthesis and Characterization. Syntheses of the axially substituted complexes were based on [Ru(qpy)(Cl)$_2$], which is analogous to the [Ru(dpp)(Cl)$_2$] complex reported by Thummel et al. and was made according to their procedure, starting from [RuCl$_3$·3H$_2$O].[26] Following dissolution of the complex in deuterated DMSO for NMR characterization, it was possible to observe exchange of the chloride ligands for DMSO, as previously reported.

Complexes **1** and **2** were prepared under air-free conditions in the dark. 1 equiv of [Ru(qpy)(Cl)$_2$] and 1 equiv of AgBF$_4$ (for **2**, excess AgBF$_4$ was used) were placed under a nitrogen atmosphere with the container covered in aluminum foil. Anhydrous acetonitrile was added and the mixture was heated at reflux overnight. Complex **2** formed as a minor byproduct in the synthesis of **1**; the complexes were purified by size exclusion chromatography using acetonitrile/water (1:1) as the eluent. After drying in vacuo, the products were obtained: **1** as a purple powder in moderate (50%) yield and **2** as a red powder in excellent (85%) yield. Although the AgBF$_4$ was weighed out as carefully as possible and the reaction was repeated a number of times, it was not possible to improve the yield of **1** as the formation of **2** was unavoidable.

Complex **3** was synthesized by heating excess 4-vinylpyridine and [Ru(qpy)(Cl)$_2$] at reflux in an ethanol−water mixture for 2 days. The complex was purified by size-exclusion chromatography using methanol/water (1:1) as the eluent. Evaporation of the solvent afforded a dark-purple powder in good (75%) yield.

The complexes were characterized by using ESI−MS, ^{1}H NMR spectroscopy, and elemental analysis. A molecular mass peak corresponding to [M]$^+$ was observed for **1**, where the ruthenium atom was in the +3 oxidation state. For complexes **1** and **2**, it was possible to observe the peak corresponding to the loss of one anion; a peak assigned to the loss of both anions was present for all complexes. A peak corresponding to the loss of one anion and one vinylpyridine ligand was present in the ESI−MS spectrum of **3**.

Proton NMR spectra of **1** and **2** in deuterated acetonitrile, Figure 1, were assigned by using COSY spectra (data not shown) starting with H^a (see Supporting Information Scheme S2), which has a characteristic shift as it points toward the Ru(II) center. The signals of **1** are shifted downfield compared with those of **2** due to the electron-withdrawing nature of the chloride ligand. If an acetonitrile solution of **1** was left to stand

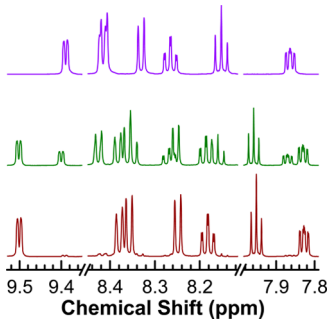

Figure 1. ^{1}H NMR spectra of **1** and **2** measured in CD$_3$CN. (top) Fresh solution of **2**, (middle) aged solution of **1**, and (bottom) **1**.

DOI: 10.1021/acs.jpca.6b00317
J. Phys. Chem. A 2016, 120, 1845−1852

for a number of hours, additional features appeared in the ^{1}H NMR spectrum. Comparison of the spectrum of this aged solution with spectra of fresh solutions of **1** and **2** reveals that **1** converts to **2** by exchanging the chloride ligand for acetonitrile over time (Figure 1).

The ^{1}H NMR spectrum of **3** in deuterated acetonitrile (Figure S1), exhibits signals characteristic for the AA′XX′ pattern of vinyl groups along with a strong trans-coupling (17.6 Hz) between the signal at δ 6.51 and that at 5.93 ppm. This is in agreement with observations by Thummel et al. for their [Ru(dpp)(vpy)$_2$] complex.[26] Elemental analysis confirmed the purity of complexes **1**−**3**.

Electronic Absorption Spectra. UV−visible absorption spectra for complexes **1**−**3** in acetonitrile are presented in Figure 2. In the visible spectral region, all three complexes

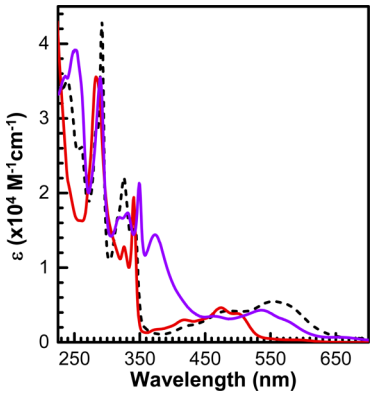

Figure 2. Molar absorptivity spectra of **1** (dashed black), **2** (red), and **3** (purple) dissolved in CH_3CN (5×10^{-5} M).

exhibit broad absorption bands as a consequence of overlapping $^1A_1 \rightarrow {}^1$MLCT transitions.[33−35] For complexes **1** and **2,** which each have only one π-acceptor ligand, the observed visible absorption bands arise from $t_{2g} \rightarrow \pi^*$(qpy) transitions. In contrast, **3** has two π-acceptor ligands and so the MLCT bands are a mix of $t_{2g} \rightarrow \pi^*$(qpy) and $t_{2g} \rightarrow \pi^*$(vpy) transitions. The MLCT absorbance of **2** is narrower and blue-shifted with respect to **1** and **3**. The absorption profile of **3** in the MLCT region (~350−700 nm) compares well with that of [Ru(dpp)(vpy)$_2$]$^{2+}$ first reported by Thummel et al.[26] High-energy absorptions are also observed in the spectra of **1** and **2** due to $\pi \rightarrow \pi^*$ and n $\rightarrow \pi^*$ transitions ascribed to the qpy ligand with peaks centered around 290, 325, and 340 nm. In the spectrum of **3**, the broad absorption centered at 375 nm is due to the vinylpyridine ligand. Absorption maxima and molar extinction coefficients are summarized in Table 1.

Steady-State Emission. As previously observed for related complexes,[26] **1**−**3** in fluid solution are nonluminescent at room temperature due to competitive nonradiative decay pathways arising from the quaterpyridine acceptor ligand. In 4:1 ethanol/methanol frozen glasses at 77 K, all three complexes become weakly emissive upon visible MLCT excitation, with results summarized in Table 2 and Figure 3. The luminescence spectra

Table 2. Luminescence Properties of 1-3 in 77 K, 4:1 Ethanol/Methanol Glasses

complex	aux. ligands	λ_{em} (nm)[a,b,c]	τ (ns)[b,d,e,f,g,h]
1	CH_3CN, Cl	770	205
2	CH_3CN	685	triexp
3	vpy	750	277

[a]Observed ^{3}MLCT $\rightarrow {}^1A_1$ emission wavelength maximum (±1 nm). [b]Data from 5 mM, argon-saturated samples. [c]Independent of visible-light excitation wavelength. [d]$\tau = k^{-1}$. [e]Independent of visible monitoring wavelength. [f]±5% uncertainty. [g]444 nm excitation. [h]For component lifetimes and amplitudes, see Supporting Figures S5−S7 in the Supporting Information.

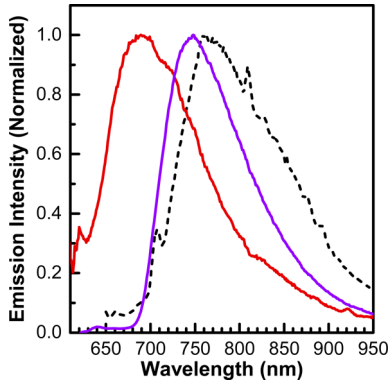

Figure 3. Normalized emission spectra recorded upon visible-light excitation of 5 mM solutions of **1** (dashed black, λ_{ex} 470 nm), **2** (red, λ_{ex} 475 nm), and **3** (purple, λ_{ex} 465 nm) in 4:1 ethanol/methanol at 77 K. Complications in baseline correction by optical interference from bubbles generated by boiling nitrogen surrounding the NMR tube used to record the spectra are depicted in Figures S2−S4 in the SI.

of the complexes exhibit broad, featureless bands that generally lie between 600 and 1000 nm with maxima at 770, 690, and 750 nm for **1**, **2**, and **3**, respectively, consistent with phosphorescent MLCT excited states, for example, ^{3}[Ru^{III}(qpy$^{\bullet-}$)(vpy)$_2$]$^{2+*}$. Excitation spectra were overlays of MLCT absorption spectra for each complex. Excitation at multiple wavelengths spanning the visible absorptions resulted in qualitatively similar photoluminescence spectra, Figures S2−S4, with the emission intensities proportional to the relative absorbances at those wavelengths and notable decreases in emission upon UV/near-UV $\pi \rightarrow \pi^*$ excitation consistent with less than unity interconversion between ligand-based $\pi\pi^*$ and the lowest MLCT states.

The emission energy for chloro complex **1** occurs at the lowest energy of the three complexes (Table 2 and Figure 3), consistent with Cl$^-$ stabilization by electron donation to Ru^{III} in

Table 1. Electronic Absorption Data for 1−3 in CH_3CN

complex	aux. ligands	λ_{max}, nm (ε x 10^3, M^{-1}cm^{-1})[a,b]
1	CH_3CN, Cl	575 sh (46.5), 550 (49.9), 480 (38.3), 420 (19.9), 340 (144.6), 325 (200.6), 316 sh (152.2), 292 (392.6), 283 sh (260.9), 260 (239.3), 239 (320.7)
2	CH_3CN	500 (3.83), 475 (4.63), 420 (3.00), 375 (14.35), 341 (19.42), 326 (12.80), 291 sh (27.30), 283 (35.55), 240 sh (19.95)
3	vpy	575 sh (2.89), 536 (4.31), 465 (3.48), 375 (14.35), 349 (21.30), 332 (17.33), 318 (16.68), 290 (35.46), 251 (39.17), 236 (35.66)

[a]$^1A_1 \rightarrow {}^1$MLCT absorption maxima (±1 nm). [b]Data from 5×10^{-5} M samples.

DOI: 10.1021/acs.jpca.6b00317
J. Phys. Chem. A 2016, 120, 1845−1852

the $Ru^{III}(qpy•^{-})$-based MLCT excited state. Similarly, the highest energy emission is observed for the bis-CH_3CN complex due to the weak electron-donating ability of the nitrile ligands. In contrast with related Ru(II) polypyridyl complexes like $[Ru(bpy)_3]^{2+}$,[36] well-defined vibronic structure is not observed in the low-temperature spectra.

Emission Spectral Fitting. Parameters derived from single-mode, Franck−Condon analysis (see Experimental Section) of emission spectra for **2** and **3** are shown in Table 3, with the corresponding fits shown in Supporting Figures S8 and S9 in the Supporting Information. In the fits, the quantum spacing was fixed at 1350 cm^{-1}. Spectral fitting was not possible for **1** due to inaccurate background subtraction of the data.

Table 3. Emission Spectral Fitting Parameters for the MLCT Excited States of 2 and 3 in 77 K[a]

complex	aux. ligands	E_0 (cm^{-1})	S_M	$\hbar\omega_M$ (cm^{-1})	fwhm (cm^{-1})
2	CH_3CN	14 560	0.84	1350	1809
3	vpy	13 300	0.54	1350	1533

[a]4:1 ethanol/methanol glasses.

With the limited data set, detailed correlations are not possible, but it is notable that E_o and the excited-state energy gap are decreased for the vpy complex, as expected for the ligand effects of the auxiliary trans ligands. The decrease in energy gap is paralleled by decreases in the electron-vibrational coupling constant, S_M, and intramolecular reorganization energy, $S_M\hbar\omega_M$,[32] the latter by 405 cm^{-1}.

Time-Resolved Emission. Excited-state decay for complexes **1**−**3** in 4:1 ethanol/methanol glasses at 77 K was monitored by time-correlated single-photon counting following visible MLCT excitation (Supporting Figures S5−S7). Emission decays for **1** and **3** were first-order but were complex and monitoring-wavelength-dependent for **2**, perhaps due to inefficient $\pi\pi^*$-MLCT interconversion. The lifetimes, listed in Table 2, are significantly shorter than those for analogous Ru(II) polypyridyl complexes with 2,2′-bipy as the acceptor ligand.[37,38] Excited-state lifetimes are dictated by the sum of lifetimes for radiative ($\tau_r = 1/k_r$) and nonradiative decay ($\tau_{nr} = 1/k_{nr}$) with $\tau = (k_r + k_{nr})^{-1}$ and, given the relatively weak emission intensities, $\tau = k_{nr}^{-1}$. For related Ru(II)-bpy complexes, in the absence of significant contributions to k_{nr} from dd state decay, linear correlations are commonly observed between $\ln(k_{nr})$ and E_0, consistent with the energy gap law.[39−42] Again, there are too few data to explore a related correlation for the qpy complexes, but the emission decay kinetics are qualitatively similar for **1** and **3** and, given the weak emissions, there may be a significant contribution to nonradiative decay through population and decay from low-lying dd states accessible in the strained coordination environment of the qpy ligand.

Electrochemistry. The redox properties of **1**−**3** were investigated at room temperature in acetonitrile by cyclic voltammetry measurements (Figure 4). $E_{1/2}$ values for the $Ru^{III/II}$ couples versus Ag/AgCl reference (0.209 V vs NHE) are listed in Table 4. Again, the $E_{1/2}$ values vary as expected with the nature of the electron-donating and π^*-acceptor ability of the auxiliary trans ligands. For complexes **1** and **2**, the Ru(III/II) redox wave was fully reversible with the $E_{1/2}$ of **1** decreased in potential relative to **2** due to the increased electron-donating nature of chloride relative to acetonitrile. The CV of **3** exhibited behavior consistent with a chemical reaction induced by oxidation of **3** at the electrode, based on literature precedent, presumably involving polymerization of the vinyl ligands or oxidatively induced reaction with the glassy carbon electrode, leading to irreversibility particularly at slower scan rates. Visual inspection of the glassy carbon working electrode following multiple scans with **3** in solution revealed the formation of a film, providing further indication of polymerization/surface reaction occurring at the glassy carbon electrode surface.

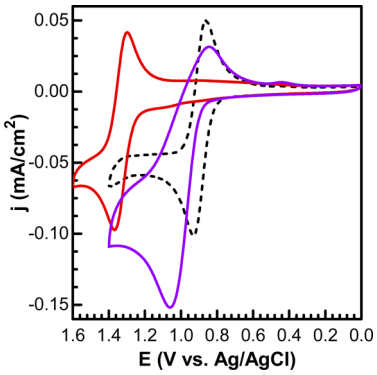

Figure 4. Cyclic voltammograms of **1** (dashed black), **2** (red), and **3** (purple) in acetonitrile 0.1 M in $[N(t\text{-}C_4H_9)_4]PF_6$ (TBAPF$_6$) at a scan rate of ν = 10 mV s^{-1}: glassy carbon electrode, Pt counter, vs Ag/AgCl (3 M NaCl, 0.209 V vs NHE); starting potential: 0 V vs Ag/AgCl; 1st scans shown.

Table 4. $E_{1/2}$ Values for 1−3 in CH_3CN

complex	aux. ligands	$E_{1/2}$ (V)[a,b,c]
1	CH_3CN, Cl	0.90
2	CH_3CN	1.33
3	Vpy	0.96

[a]$Ru^{III/II}$ reduction potentials measured in acetonitrile containing 0.1 M TBAPF$_6$ with a glassy carbon working electrode at 10 mV s^{-1}. [b]Potentials reported relative to Ag/AgCl. [c]Air-saturated solutions.

Upon dissolution of **1** in 0.1 M TFA solution, redox couples (Supporting Figure S10) appear at $E_{1/2}$ = 0.58, 0.87, and 1.09 V in cyclic voltammograms (CVs) in the range 0−1.4 V versus Ag/AgCl. By analogy to the related polypyridyl complex *trans*-$[Ru(bpy)_2(OH_2)_2]^{2+}$,[20,21,43−47] these waves are attributable to initial solvolysis to give the diaqua complex, $[Ru(qpy)(OH_2)_2]^{2+}$, eq 2, and the redox couples in eqs 3a−3c. In this sequence, initial $H_2O-Ru^{II}-OH_2^{2+}$ oxidation to $H_2O-Ru^{III}-OH_2^{3+}$ is followed by a kinetically inhibited $1e^-/2H^+$ oxidation of $H_2O-Ru^{III}-OH_2^{3+}$ to $H_2O-Ru^{IV}=O^{2+}$, followed by further $2e^-/2H^+$ oxidation to *trans*-$O=Ru^{VI}=O^{2+}$. Three redox couples are also observed for **2** in 0.1 M TFA and, as shown in Figure 5, the slight shifts in peak potentials upon successive scans point to the final stages of substitutional equilibration. The final CV after 20 scans closely resembled that reported by Che et al. for $[Ru(qpy)(OH_2)_2]^{2+}$.[20] For $[Ru^{II}(qpy)(vpy)_2]^{2+}$ in 0.1 M TFA, a Ru(III/II) wave is observed at $E_{1/2}(Ru^{III/II})$ = 0.98 V versus Ag/AgCl at either glassy carbon or boron-doped diamond working electrodes, a value nearly identical to the value observed in CH_3CN (0.96 V vs Ag/AgCl). It is notable that the Ru(III/II) wave is more reversible in wave shape in 0.1 M TFA than in CH_3CN, consistent with CH_3CN acting as an inert solvent for sustaining C−C bond formation with the surface or during oxidative polymerization of the vinyl ligand. In 0.1 M TFA, an additional oxidative wave for **3** appeared at 0.54 V (Supporting Figure S11) at glassy carbon working

DOI: 10.1021/acs.jpca.6b00317
J. Phys. Chem. A 2016, 120, 1845−1852

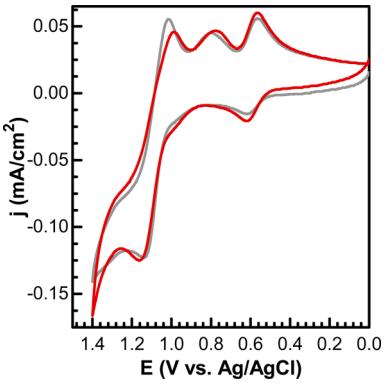

Figure 5. Cyclic voltammograms for **2** in air-saturated 0.1 M TFA, illustrating potential shifts between the 1st (gray) and 20th (red) scans. Working: glassy carbon; counter: Pt wire; reference: Ag/AgCl (3 M NaCl, 0.209 V vs NHE); starting potential: 0 V vs Ag/AgCl.

electrodes characteristic of surface binding. To probe the importance of the electrode surface, we carried out CV scans at a boron-doped diamond (BDD) working electrode. At BDD, the wave at 0.54 V did not appear in CV scans and the capacitive background was significantly reduced, consistent with its known inert behavior as an electrode.[48] $E_{1/2}$ values for $Ru^{III/II}$ couples versus Ag/AgCl reference (0.209 V vs NHE) in 0.1 M TFA solution are listed in Table 5.

$$[Ru^{II}(qpy)(CH_3CN)_2]^{2+} + 2H_2O \rightarrow [Ru^{II}(qpy)(OH_2)_2]^{2+} + 2CH_3CN \quad (2)$$

$$[Ru^{II}(qpy)(OH_2)_2]^{2+} \xrightarrow{-e^-} [Ru^{III}(qpy)(OH_2)_2]^{3+} \quad (3a)$$

$$[Ru^{III}(qpy)(OH_2)_2]^{3+} \xrightarrow{-e^-,-2H^+} [Ru^{IV}(qpy)(O)(OH_2)_2]^{2+} \quad (3b)$$

$$[Ru^{IV}(qpy)(O)(OH_2)_2]^{2+} \xrightarrow{-2e^-,-2H^+} [Ru^{VI}(qpy)(O)_2]^{2+} \quad (3c)$$

Table 5. $E_{1/2}$ Values for 1−3 in 0.1 M TFA[a,b]

	$E_{1/2}$ (V)		
complex	$Ru^{II/III}$	$Ru^{III/IV}$	$Ru^{VI/IV}$
1	0.58	0.87	1.09
2	0.59	0.82	1.09
3	0.98		

[a]In 0.1 M TFA with a glassy carbon working electrode and Pt counter electrode at 10 mV s^{-1}. [b]$E_{1/2}$ values versus Ag/AgCl.

CONCLUSIONS

Three complexes based on the {Ru(qpy)LL′} motif have been synthesized and characterized. They are broad MLCT light absorbers and nonluminescent at room temperature but do emit weakly in an ethanol/methanol glass at 77 K. The mixed ligand complex **1** exhibits the most red-shifted absorption and emission spectra and lowest $Ru^{III/II}$ redox potential due to the electron-donating nature of the chloride ligand. Although ligand exchange is not observed for the vinylpyridine-derivatized complex **3**, dissolution of **1** or **2** in 0.1 M trifluoroacetic acid promotes replacement of the acetonitrile and, for **2**, chloride ligands by water to give the corresponding diaqua complex, $[Ru^{II}(qpy)(OH_2)_2]^{2+}$. By analogy to *trans*-$[Ru(bpy)_2(OH_2)_2]^{2+}$, the diaqua complex undergoes successive $1e^-$ oxidation to $[Ru^{III}(qpy)(OH_2)_2]^{3+}$, followed by $2e^-/2H^+$ oxidation to $[Ru^{IV}(qpy)(O)(OH_2)]^{2+}$ and further $2e^-/2H^+$ oxidation to $[Ru^{VI}(qpy)(O)_2]^{2+}$. Its abilities as a water oxidation catalyst are currently under investigation.

ASSOCIATED CONTENT

Supporting Information

The Supporting Information is available free of charge on the ACS Publications website at DOI: 10.1021/acs.jpca.6b00317.

Proton assignments (H^a-H^g) for the qpy ligand, the ^1H NMR spectrum of **3** along with the synthetic scheme, excitation-dependent emission spectra, emission spectral fits, time-resolved emission data with corresponding fits, and cyclic voltammograms for complexes **1**−**3**. (PDF)

AUTHOR INFORMATION

Corresponding Author

*E-mail: tjmeyer@unc.edu.

Author Contributions

The manuscript was written through contributions of all authors. All authors have given approval to the final version of the manuscript.

Notes

The authors declare no competing financial interest.

ACKNOWLEDGMENTS

This research was supported by the UNC EFRC: Center for Solar Fuels, an Energy Frontier Research Center funded by the U.S. Department of Energy, Office of Science, Office of Basic Energy Sciences, under Award Number DE-SC0001011. The Swiss National Science Foundation is acknowledged for supporting J.A.R. with an individual Early Postdoc Mobility Fellowship. D.L.A. acknowledges support from an individual fellowship from the Department of Energy Office of Science Graduate Fellowship Program (DOE SCGF), made possible in part by the American Recovery and Reinvestment Act of 2009, administered by ORISE-ORAU under Contract No. DE-AC05-06OR23100.

ABBREVIATIONS

qpy, 2,2′:6′,2″:6″,2‴-quaterpyridine; MLCT, metal-to-ligand charge transfer; TFA, trifluoroacetic acid; WOC, water oxidation catalyst; dpp, 2,9-di(pyrid-2′-yl)-1,10-phenanthroline; pic, picoline = *para*-methylpyridine; vpy, *para*-vinylpyridine; DMSO, dimethyl sulfoxide; ESI, electrospray ionization; NMR, nuclear magnetic resonance; MS, mass spectrometry; COSY, correlation spectroscopy; CV, cyclic voltammogram; bpy, 2,2′-bipyridine

REFERENCES

(1) Alibabaei, L.; Luo, H. L.; House, R. L.; Hoertz, P. G.; Lopez, R.; Meyer, T. J. Applications of Metal Oxide Materials in Dye Sensitized Photoelectrosynthesis Cells for Making Solar Fuels: Let the Molecules Do the Work. *J. Mater. Chem. A* **2013**, *1*, 4133−4145.

(2) Alstrum-Acevedo, J. H.; Brennaman, M. K.; Meyer, T. J. Chemical Approaches to Artificial Photosynthesis. 2. *Inorg. Chem.* **2005**, *44*, 6802−6827.

DOI: 10.1021/acs.jpca.6b00317
J. Phys. Chem. A 2016, 120, 1845−1852

(3) Concepcion, J. J.; House, R. L.; Papanikolas, J. M.; Meyer, T. J. Chemical Approaches to Artificial Photosynthesis. *Proc. Natl. Acad. Sci. U. S. A.* **2012**, *109*, 15560−15564.
(4) Gust, D.; Moore, T. A.; Moore, A. L. Solar Fuels via Artificial Photosynthesis. *Acc. Chem. Res.* **2009**, *42*, 1890−1898.
(5) Meyer, T. J. Chemical Approaches to Artificial Photosynthesis. *Acc. Chem. Res.* **1989**, *22*, 163−170.
(6) Song, W. J.; Chen, Z. F.; Brennaman, M. K.; Concepcion, J. J.; Patrocinio, A. O. T.; Iha, N. Y. M.; Meyer, T. J. Making Solar Fuels by Artificial Photosynthesis. *Pure Appl. Chem.* **2011**, *83*, 749−768.
(7) Walter, M. G.; Warren, E. L.; McKone, J. R.; Boettcher, S. W.; Mi, Q. X.; Santori, E. A.; Lewis, N. S. Solar Water Splitting Cells. *Chem. Rev.* **2010**, *110*, 6446−6473.
(8) Dau, H.; Limberg, C.; Reier, T.; Risch, M.; Roggan, S.; Strasser, P. The Mechanism of Water Oxidation: From Electrolysis via Homogeneous to Biological Catalysis. *ChemCatChem* **2010**, *2*, 724−761.
(9) Duan, L.; Tong, L.; Xu, Y.; Sun, L. Visible Light-Driven Water Oxidation-from Molecular Catalysts to Photoelectrochemical Cells. *Energy Environ. Sci.* **2011**, *4*, 3296−3313.
(10) Kärkäs, M. D.; Verho, O.; Johnston, E. V.; Åkermark, B. Artificial Photosynthesis: Molecular Systems for Catalytic Water Oxidation. *Chem. Rev.* **2014**, *114*, 11863−12001.
(11) Deng, Z.; Tseng, H.-W.; Zong, R.; Wang, D.; Thummel, R. Preparation and Study of a Family of Dinuclear Ru(II) Complexes That Catalyze the Decomposition of Water. *Inorg. Chem.* **2008**, *47*, 1835−1848.
(12) Duan, L.; Araujo, C. M.; Ahlquist, M. S. G.; Sun, L. Highly Efficient and Robust Molecular Ruthenium Catalysts for Water Oxidation. *Proc. Natl. Acad. Sci. U. S. A.* **2012**, *109*, 15584−15588.
(13) Duan, L.; Bozoglian, F.; Mandal, S.; Stewart, B.; Privalov, T.; Llobet, A.; Sun, L. A Molecular Ruthenium Catalyst with Water-Oxidation Activity Comparable to that of Photosystem II. *Nat. Chem.* **2012**, *4*, 418−423.
(14) Kaveevivitchai, N.; Kohler, L.; Zong, R.; El Ojaimi, M.; Mehta, N.; Thummel, R. P. A Ru(II) Bis-terpyridine-like Complex that Catalyzes Water Oxidation: The Influence of Steric Strain. *Inorg. Chem.* **2013**, *52*, 10615−10622.
(15) Muckerman, J. T.; Kowalczyk, M.; Badiei, Y. M.; Polyansky, D. E.; Concepcion, J. J.; Zong, R.; Thummel, R. P.; Fujita, E. New Water Oxidation Chemistry of a Seven-Coordinate Ruthenium Complex with a Tetradentate Polypyridyl Ligand. *Inorg. Chem.* **2014**, *53*, 6904−6913.
(16) Staehle, R.; Tong, L.; Wang, L.; Duan, L.; Fischer, A.; Ahlquist, M. S. G.; Sun, L.; Rau, S. Water Oxidation Catalyzed by Mononuclear Ruthenium Complexes with a 2,2′-Bipyridine-6,6′-dicarboxylate (bda) Ligand: How Ligand Environment Influences the Catalytic Behavior. *Inorg. Chem.* **2014**, *53*, 1307−1319.
(17) Renouard, T.; Fallahpour, R. A.; Nazeeruddin, M. K.; Humphry-Baker, R.; Gorelsky, S. I.; Lever, A. B. P.; Grätzel, M. Novel Ruthenium Sensitizers Containing Functionalized Hybrid Tetradentate Ligands: Synthesis, Characterization, and INDO/S Analysis. *Inorg. Chem.* **2002**, *41*, 367−378.
(18) Tong, L.; Zong, R.; Zhou, R.; Kaveevivitchai, N.; Zhang, G.; Thummel, R. P. Ruthenium Catalysts for Water Oxidation Involving Tetradentate Polypyridine-Type Ligands. *Faraday Discuss.* **2015**, *185*, 87−104.
(19) Liu, Y.; Ng, S.-M.; Yiu, S.-M.; Lam, W. W. Y.; Wei, X.-G.; Lau, K.-C.; Lau, T.-C. Catalytic Water Oxidation by Ruthenium(II) Quaterpyridine (qpy) Complexes: Evidence for Ruthenium(III) qpy-N,N‴-dioxide as the Real Catalysts. *Angew. Chem., Int. Ed.* **2014**, *53*, 14468−14471.
(20) Chan, C.-W.; Lai, T.-F.; Che, C.-M. Electrochemical Oxidation of Diaquaruthenium(II) Complexes of Quaterpyridines and Crystal Structure of $[RuL^1(PPh_3)_2][ClO_4]_2$ (L^1= 3″,5,5′,5‴-tetramethyl-2,2′:6′,2″:6″,2‴-quaterpyridine). *J. Chem. Soc., Dalton Trans.* **1994**, 895−899.
(21) Harrison, D. P.; Lapides, A. M.; Binstead, R. A.; Concepcion, J. J.; Méndez, M. A.; Torelli, D. A.; Templeton, J. L.; Meyer, T. J. Coordination Chemistry of Single-Site Catalyst Precursors in Reductively Electropolymerized Vinylbipyridine Films. *Inorg. Chem.* **2013**, *52*, 4747−4749.
(22) Ghosh, P.; Spiro, T. G. Photoelectrochemistry of Tris-(bipyridyl)ruthenium(II) Covalently Attached to n-type Tin(IV) Oxide. *J. Am. Chem. Soc.* **1980**, *102*, 5543−5549.
(23) Abruña, H. D.; Denisevich, P.; Umaña, M.; Meyer, T. J.; Murray, R. W. Rectifying Interfaces Using Two-Layer Films of Electrochemically Polymerized Vinylpyridine and Vinylbipyridine Complexes of Ruthenium and Iron on Electrodes. *J. Am. Chem. Soc.* **1981**, *103*, 1−5.
(24) Ashford, D. L.; Lapides, A. M.; Vannucci, A. K.; Hanson, K.; Torelli, D. A.; Harrison, D. P.; Templeton, J. L.; Meyer, T. J. Water Oxidation by an Electropolymerized Catalyst on Derivatized Mesoporous Metal Oxide Electrodes. *J. Am. Chem. Soc.* **2014**, *136*, 6578−6581.
(25) Hu, Y.-Z.; Xiang, Q.; Thummel, R. P. Bi-1,10-phenanthrolines and Their Mononuclear Ru(II) Complexes. *Inorg. Chem.* **2002**, *41*, 3423−3428.
(26) Zong, R.; Wang, B.; Thummel, R. P. *trans*-$[Ru^{II}(dpp)Cl_2]$: A Convenient Reagent for the Preparation of Heteroleptic Ru(dpp) Complexes, Where dpp Is 2,9-Di(pyrid-2′-yl)-1,10-phenanthroline. *Inorg. Chem.* **2012**, *51*, 3179−3185.
(27) Parker, C. A.; Rees, W. T. Correction of Fluorescence Spectra and Measurement of Fluorescence Quantum Efficiency. *Analyst* **1960**, *85*, 587−600.
(28) Claude, J. P. Ph.D. Dissertation, University of North Carolina at Chapel Hill, 1995.
(29) Kestell, J. D.; Williams, Z. L.; Stultz, L. K.; Claude, J. P. Medium Dependence of Intramolecular Vibrational Modes Coupled to MLCT Transitions in Metal Polypyridyl Complexes. *J. Phys. Chem. A* **2002**, *106*, 5768−5778.
(30) Kober, E. M.; Caspar, J. V.; Lumpkin, R. S.; Meyer, T. J. Application of the Energy Gap Law to Excited-State Decay of Osmium(II)-Polypyridine Complexes: Calculation of Relative Nonradiative Decay Rates from Emission Spectral Profiles. *J. Phys. Chem.* **1986**, *90*, 3722−3734.
(31) Claude, J. P.; Meyer, T. J. Temperature Dependence of Nonradiative Decay. *J. Phys. Chem.* **1995**, *99*, 51−54.
(32) Ito, A.; Meyer, T. J. The Golden Rule. Application for Fun and Profit in Electron Transfer, Energy Transfer, and Excited-State Decay. *Phys. Chem. Chem. Phys.* **2012**, *14*, 13731−13745.
(33) Kober, E. M.; Meyer, T. J. Concerning the Absorption Spectra of the Ions $M(bpy)_3^{2+}$ (M = Fe, Ru, Os; bpy = 2,2′-bipyridine). *Inorg. Chem.* **1982**, *21*, 3967−3977.
(34) Strouse, G. F.; Anderson, P. A.; Schoonover, J. R.; Meyer, T. J.; Keene, F. R. Synthesis of Polypyridyl Complexes of Ruthenium(II) Containing Three Different Bidentate Ligands. *Inorg. Chem.* **1992**, *31*, 3004−3006.
(35) Anderson, P. A.; Strouse, G. F.; Treadway, J. A.; Keene, F. R.; Meyer, T. J. Black MLCT Absorbers. *Inorg. Chem.* **1994**, *33*, 3863−3864.
(36) Barigelletti, F.; Belser, P.; Von Zelewsky, A.; Juris, A.; Balzani, V. Luminescence of Mixed-Ligand Polypyridine-Ruthenium(II) Complexes in the Temperature Range 84−250 K. Interligand Interactions and Viscosity Effects on Radiationless Processes. *J. Phys. Chem.* **1985**, *89*, 3680−3684.
(37) Campagna, S.; Puntoriero, F.; Nastasi, F.; Bergamini, G.; Balzani, V. In *Photochemistry and Photophysics of Coordination Compounds I*; Balzani, V., Campagna, S., Eds.; Springer: Berlin, 2007; Vol. *280*, pp 117−214.
(38) Lumpkin, R. S.; Kober, E. M.; Worl, L. A.; Murtaza, Z.; Meyer, T. J. Metal-to-Ligand Charge-Transfer (MLCT) Photochemistry. Experimental Evidence for the Participation of a Higher Lying MLCT State in Polypyridyl Complexes of Ruthenium(II) and Osmium(II). *J. Phys. Chem.* **1990**, *94*, 239−243.
(39) Caspar, J. V.; Sullivan, B. P.; Kober, E. M.; Meyer, T. J. Application of the Energy Gap Law to the Decay of Charge Transfer Excited States, Solvent Effects. *Chem. Phys. Lett.* **1982**, *91*, 91−95.

DOI: 10.1021/acs.jpca.6b00317
J. Phys. Chem. A 2016, 120, 1845−1852

(40) Caspar, J. V.; Kober, E. M.; Sullivan, B. P.; Meyer, T. J. Application of the Energy Gap Law to the Decay of Charge-Transfer Excited States. *J. Am. Chem. Soc.* **1982**, *104*, 630−632.
(41) Caspar, J. V.; Meyer, T. J. Application of the Energy Gap Law to Nonradiative, Excited-State Decay. *J. Phys. Chem.* **1983**, *87*, 952−957.
(42) Meyer, T. J. Photochemistry of Metal Coordination Complexes: Metal to Ligand Charge Transfer Excited States. *Pure Appl. Chem.* **1986**, *58*, 1193−1206.
(43) Navarro, M.; De Giovani, W. F.; Romero, J. R. Electrocatalytic Oxidation of Alcohols and Diols using Polypyridyl Complexes of Ruthenium. Effect of the Redox Potential on Selectivity. *J. Mol. Catal. A: Chem.* **1998**, *135*, 249−256.
(44) Moyer, B. A.; Meyer, T. J. Oxobis(2,2′-bipyridine)-pyridineruthenium(IV) ion, $[(bpy)_2(py)Ru{=}O]^{2+}$. *J. Am. Chem. Soc.* **1978**, *100*, 3601−3603.
(45) Durham, B.; Wilson, S. R.; Hodgson, D. J.; Meyer, T. J. Cis-Trans Photoisomerization in $Ru(bpy)_2(OH_2)_2^{2+}$. Crystal Structure of *trans*-$[Ru(bpy)_2(OH_2)\ (OH)](ClO_4)_2$. *J. Am. Chem. Soc.* **1980**, *102*, 600−607.
(46) Dobson, J. C.; Meyer, T. J. Redox Properties and Ligand Loss Chemistry in Aqua/Hydroxo/Oxo Complexes Derived from *cis*- and *trans*-$[(bpy)_2Ru^{II}(OH_2)_2]^{2+}$. *Inorg. Chem.* **1988**, *27*, 3283−3291.
(47) Song, N.; Concepcion, J. J.; Binstead, R. A.; Rudd, J. A.; Vannucci, A. K.; Dares, C. J.; Coggins, M. K.; Meyer, T. J. Base-Enhanced Catalytic Water Oxidation by a Carboxylate−Bipyridine Ru(II) Complex. *Proc. Natl. Acad. Sci. U. S. A.* **2015**, *112*, 4935−4940.
(48) Luong, J. H. T.; Male, K. B.; Glennon, J. D. Boron-Doped Diamond Electrode: Synthesis, Characterization, Functionalization and Analytical Applications. *Analyst* **2009**, *134*, 1965−1979.

DOI: 10.1021/acs.jpca.6b00317
J. Phys. Chem. A 2016, 120, 1845−1852